Co-targeting of convergent nucleotide biosynthetic pathways for leukemia eradication

David A. Nathanson,[1,2] Amanda L. Armijo,[1,2] Michelle Tom,[1,2] Zheng Li,[1,2] Elizabeth Dimitrova,[1,2] Wayne R. Austin,[1,2] Julian Nomme,[7] Dean O. Campbell,[1,2] Lisa Ta,[1,2] Thuc M. Le,[1,2] Jason T. Lee,[1,2] Ryan Darvish,[1,2] Ari Gordin,[1,2] Liu Wei,[1,2] Hsiang-I Liao,[1,2] Moses Wilks,[3] Colette Martin,[1,2] Saman Sadeghi,[1,2] Jennifer M. Murphy,[1,2] Nidal Boulos,[8] Michael E. Phelps,[1,2] Kym F. Faull,[4] Harvey R. Herschman,[1,2,5] Michael E. Jung,[6] Johannes Czernin,[1,2] Arnon Lavie,[7] and Caius G. Radu[1,2]

[1]Department of Molecular and Medical Pharmacology; [2]Ahmanson Translational Imaging Division;
[3]Department of Biomathematics; [4]The Pasarow Mass Spectrometry Laboratory, Department of Psychiatry and Biobehavioral Sciences and the Semel Institute for Neuroscience and Human Behavior; [5]Department of Biological Chemistry; and [6]Department of Chemistry and Biochemistry, University of California, Los Angeles, Los Angeles, CA 90095
[7]Department of Biochemistry and Molecular Genetics, University of Illinois at Chicago, Chicago, IL 60607
[8]Department of Developmental Neurobiology, St. Jude Children's Research Hospital, Memphis, TN, 38105

Pharmacological targeting of metabolic processes in cancer must overcome redundancy in biosynthetic pathways. Deoxycytidine (dC) triphosphate (dCTP) can be produced both by the de novo pathway (DNP) and by the nucleoside salvage pathway (NSP). However, the role of the NSP in dCTP production and DNA synthesis in cancer cells is currently not well understood. We show that acute lymphoblastic leukemia (ALL) cells avoid lethal replication stress after thymidine (dT)–induced inhibition of DNP dCTP synthesis by switching to NSP–mediated dCTP production. The metabolic switch in dCTP production triggered by DNP inhibition is accompanied by NSP up-regulation and can be prevented using DI–39, a new high–affinity small-molecule inhibitor of the NSP rate-limiting enzyme dC kinase (dCK). Positron emission tomography (PET) imaging was useful for following both the duration and degree of dCK inhibition by DI–39 treatment in vivo, thus providing a companion pharmacodynamic biomarker. Pharmacological co-targeting of the DNP with dT and the NSP with DI–39 was efficacious against ALL models in mice, without detectable host toxicity. These findings advance our understanding of nucleotide metabolism in leukemic cells, and identify dCTP biosynthesis as a potential new therapeutic target for metabolic interventions in ALL and possibly other hematological malignancies.

CORRESPONDENCE
C.G. Radu:
CRadu@mednet.ucla.edu

The ability to reprogram cellular metabolism, a hallmark of cancer first noted long ago (Warburg et al., 1927) and recently reappreciated, is essential for tumor progression (Hanahan and Weinberg, 2011). Although cancer-initiated metabolic reprogramming processes are promising therapeutic targets (Vander Heiden, 2011), the existence of alternative, compensatory biosynthetic pathways presents a significant challenge for developing such therapies. For example, in lipid metabolism, cancer cells scavenge extracellular lipids as an alternative to energy-requiring de novo fatty acid biosynthesis (Kamphorst et al., 2011). In amino acid metabolism, glycine and serine required for tumor growth can be produced de novo and can also be scavenged from the extracellular environment (Jain et al., 2012; Maddocks et al., 2013).

Nucleotide metabolism also involves redundant and convergent biosynthetic pathways. Deoxyribonucleotide triphosphate (dNTP) pools required for DNA replication and repair can be produced by the de novo pathway (DNP) or by the nucleoside salvage pathway (NSP; Fig. 1 A; Reichard, 1988). The DNP uses glucose and amino acids to generate ribonucleotide diphosphates (NDPs), which are converted to
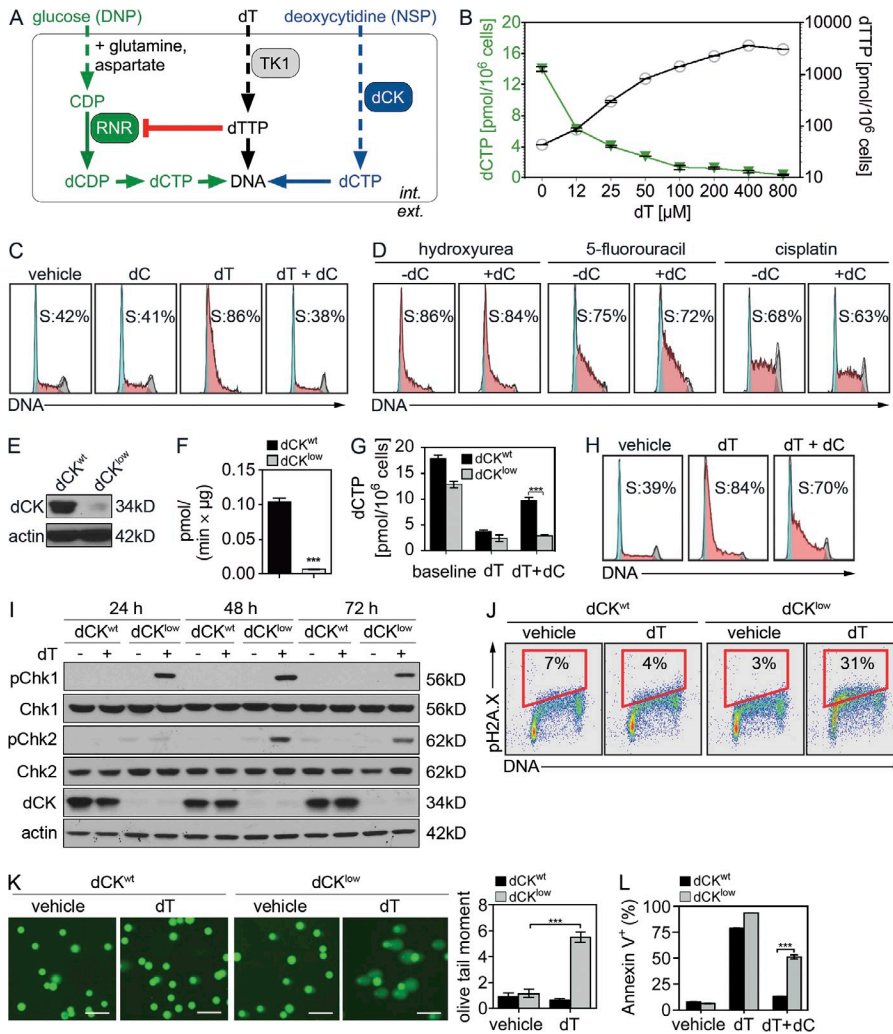
Figure 1. dC salvage via dCK prevents dT–induced lethal RS in T–ALL cells.
(A) Allosteric control of DNP dCTP production by dT via dTTP. (B) Effects of dT treatment (24 h) on dCTP and dTTP pools. Values represent mean ± SEM. (C) CEM cell cycle analysis after treatment with vehicle or 50 µM dT ± 2.5 µM dC for 24 h. (D) CEM cell cycle analysis after treatment with 50 µM hydroxyurea, 15 µM 5-fluorouracil, or 1.6 µM cisplatin for 24 h ± 2.5 µM dC. (E and F) Representative immuno-blots of dCK and actin expression (E) and dCK kinase assay (F) in CEM dCK^{wt} (scrambled shRNA) cells and dCK^{low} (shRNA against dCK) cells. Values are mean ± SEM. ***, P < 0.001. (G) dCTP levels in CEM dCK^{wt} and dCK^{low} cells treated for 24 h with vehicle or 50 µM dT ± 2.5 µM dC. Values are mean ± SEM. ***, P < 0.001. (H) Cell cycle analysis of CEM dCK^{low} cells treated with vehicle or 50 µM dT ± 2.5 µM dC for 24 h. (I) Representative immuno-blots detecting Chk1, pChk1 (Ser345), Chk2, pChk2 (Thr68), dCK, and actin in CEM dCK^{wt} and dCK^{low} cells treated with vehicle or 50 µM dT in the presence of 2.5 µM dC for 24, 48, and 72 h. (J) pH2A.X (Ser139) and DNA content (DAPI) in CEM dCK^{wt} and dCK^{low} cells treated with vehicle or 50 µM dT in the presence of 2.5 µM dC for 24 h. (K) Representative images and quantification of the COMET assay conducted on CEM dCK^{wt} and dCK^{low} cells 48 h after treatment with vehicle or 50 µM dT in the presence of 2.5 µM dC. Values represent the mean Olive Tail Moment ± SEM from 100 cells per image × 4 images/group; n = 2 independent experiments. ***, P < 0.001. Bars, 50 µm. (L) Annexin V staining of CEM dCK^{wt} and dCK^{low} cells after treatment with vehicle, 2.5 µM dC, 50 µM dT, or dC + dT for 72 h. All values are mean ± SEM from at least three replicates/data point. ***, P < 0.001. All data are representative of n = 3 independent experiments, unless indicated.

deoxyribonucleotide diphosphates (dNDPs) by ribonucleotide reductase (RNR). The same dNDPs can also be produced via the NSP (Reichard, 1988), starting with extracellular deoxyribonucleosides (dNs) which are imported in the cell via specialized transporters. The first enzymatic steps in the cytosolic NSP are catalyzed by two kinases: thymidine kinase 1 (TK1) phosphorylates thymidine (dT), while deoxycytidine (dC) kinase (dCK) phosphorylates dC, deoxyadenosine (dA), and deoxyguanosine (dG; Reichard, 1988). The relevance of these two NSP kinases for dNTP production in normal and malignant cells is yet to be defined. Because dN substrates for the NSP kinases are absent from most cell culture media, it has been assumed that the NSP is dispensable for DNA replication (Xu et al., 1995). However, recent in vivo findings have challenged this assumption. For example, we reported impaired hematopoiesis in $dCK^{-/-}$ mice due to dCTP

pool deficiency, resulting in replication stress (RS), S-phase arrest, and DNA damage in hematopoietic progenitors (Toy et al., 2010; Austin et al., 2012). Analyses of $dCK/TK1$ double-knockout mice showed that NSP-derived dCTP synthesis is required to compensate for the inhibition of de novo dCTP production (Austin et al., 2012; Fig. 1 A). The mechanism of DNP inhibition involves allosteric regulation of RNR-mediated reduction of cytidine diphosphate (CDP) to dC diphosphate (dCDP) by dT triphosphate (dTTP) produced via TK1 from endogenous dT (Austin et al., 2012; Fig. 1 A).

Production of dNTPs by the NSP may be therapeutically relevant in cancer. For example, the ability of cancer cells to switch their dCTP synthesis from the DNP to the NSP may explain why dT given as a single dCTP-depleting agent showed limited efficacy in clinical trials (Chiuten et al., 1980; Kufe et al., 1980, 1981). If correct, this hypothesis suggests
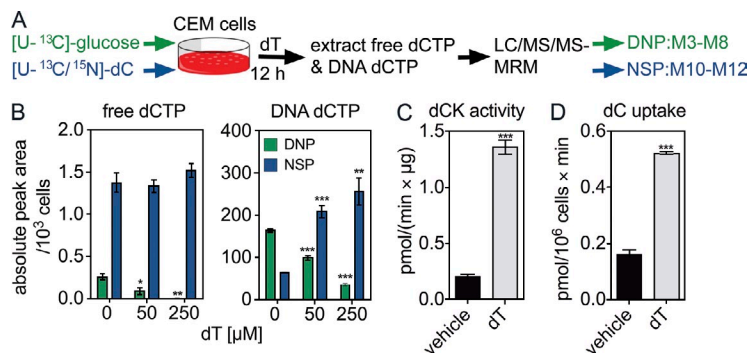
Figure 2. Treatment with dT triggers a metabolic switch to NSP–mediated dCTP biosynthesis in T-ALL cells and up-regulates the NSP. (A) Schematic of the [U-^{13}C]-glucose and [U-^{13}C/^{15}N]-dC stable isotope labeling approach used to determine the source (DNP or NSP) of the free dCTP pool and of the dCTP incorporated into the DNA of CEM cells treated with various dT concentrations. (B) dCTP derived from [U-^{13}C]-glucose (DNP) and [U-^{13}C/^{15}N]-dC (NSP) in the free dCTP pool and incorporated into the DNA of CEM cells after 12 h of incubation with stable isotope–labeled DNP and NSP precursors, in the presence or absence of dT. Values are the mean of absolute peak area/10^3 cells ± SEM. *, $P < 0.05$; **, $P < 0.01$; ***, $P < 0.001$, compared with 0 µM dT control. Data are representative of $n = 2$ independent experiments. (C) Quantification of dCK kinase activity in CEM cells at baseline and after 8 h of treatment with 50 µM dT. Data are representative of $n = 2$ independent experiments. Values are mean ± SEM. ***, $P < 0.001$. (D) Quantification of the uptake of ^{3}H-labeled dC by CEM cells at baseline and after 4 h of treatment with 50 µM dT. Data are representative of $n = 2$ independent experiments. Values represent mean ± SEM. ***, $P < 0.001$.

that a combination of dT (to inhibit DNP-mediated dCTP production) and a dCK inhibitor (to co-target dCTP production by the NSP) would be more efficacious in killing tumor cells than either treatment alone. Here, we investigate this possibility in the context of acute lymphoblastic leukemia (ALL). We demonstrate that co-targeting both de novo and salvage pathways for dCTP biosynthesis is well tolerated in mice and is efficacious in T-ALL and B-ALL models. We also describe a positron emission tomography (PET)–based assay to noninvasively monitor in vivo pharmacological targeting of dCTP biosynthesis in cancer cells.

RESULTS

dC salvage via dCK prevents dT–induced lethal RS in T-ALL cells

Treatment with dT increases cytosolic dTTP concentration, resulting in allosteric inhibition of dCTP production via the DNP (Fig. 1 A; Reichard, 1988). Accordingly, in CCRF-CEM (CEM) human T-ALL cells, dT increased dTTP and decreased dCTP in a dose-dependent manner (Fig. 1 B). Early S-arrest (Fig. 1 C) was induced by concentrations of dT as low as 50 µM, which increased dTTP ∼20-fold and reduced dCTP ∼5-fold (Fig. 1 B). Supplementation of CEM cultures with 2.5 µM dC completely prevented dT-induced S-phase arrest (Fig. 1 C). Addition of dC did not prevent S-phase arrest in CEM cells treated with the RNR inhibitor hydroxyurea, 5-FU (5-fluorouracil), or cisplatin (Fig. 1 D), indicating that dC salvage plays a specific role in counteracting dT-induced S-phase arrest.

To study the role of dCK in the prevention of dT-induced S-phase arrest by dC addition, we generated CEM dCK^{low} cells (Fig. 1 E) using a dCK-targeted shRNA vector. Knocking down dCK reduced ^{3}H-dC uptake by ∼95% (Fig. 1 F) and decreased cytosolic dCTP levels by ∼30% (Fig. 1 G) but did not perturb normal cell cycle progression (Fig. 1 H). Supplementation of cell culture media with 2.5 µM dC restored the dCTP pool in dT-treated dCK^{wt} cells to ∼55% of its baseline value but had no effect on dT-induced dCTP pool depletion in dCK^{low} cells (Fig. 1 G). Consequently, dC addition prevented dT-induced S-phase arrest only in CEM dCK^{wt} cells (Fig. 1 C) and not in CEM dCK^{low} cells (Fig. 1 H). Accordingly, in the

presence of both dT and dC, only dCK^{low} and not dCK^{wt} CEM cells displayed the following: activation of the RS response marker Chk1 phosphorylated on Ser345 (pChk1; Fig. 1 I); induction of DNA damage, as determined by activation of Chk2 phosphorylated on Thr68 (pChk2; Fig. 1 I); pH2A.X staining by flow cytometry (Fig. 1 J), as well as by comet assay (Fig. 1 K); and apoptosis (Fig. 1 L). Thus, down-regulation of dCK expression in CEM cells abolished their ability to compensate for dT-mediated inhibition of dCTP production via the DNP, resulting in dCTP depletion, stalled DNA replication, RS, DNA damage, and apoptosis.

In T-ALL cells, dT triggers a metabolic switch to NSP dCTP production and up-regulates dC salvage

To investigate the biochemical mechanism by which the NSP compensates for dT-mediated DNP inhibition, we quantified the contributions of each dCTP biosynthetic pathway to both the free cytosolic dCTP and the dCTP incorporated into the DNA. CEM cells were incubated for 12 h with [U-^{13}C]-glucose, the substrate for the DNP, and with [U-^{13}C/^{15}N]-dC, the substrate for the NSP (Fig. 2 A). Heavy isotope–labeled dCTP species were detected by combined liquid chromatography–tandem mass spectrometry in the multiple reaction-monitoring mode (LC/MS/MS-MRM). Mass additions between 3 and 8 identified dCTP produced from [U-^{13}C]-glucose via the DNP, whereas mass additions between 11 and 12 identified dCTP produced from [U-^{13}C/^{15}N]-dC via the NSP (Fig. 2 A).

In untreated CEM cells, the free dCTP pool produced from dC via the NSP over a 12-h labeling period was ∼5-fold larger than the free dCTP pool originating from glucose via the DNP (Fig. 2 B). However, ∼2.5-fold more dCTP incorporated into DNA was produced by the DNP than by the NSP (Fig. 2 B). Treatment with dT decreased dCTP production from glucose via the DNP, in both the free cytosolic and DNA dCTP pools (Fig. 2 B). Moreover, dT increased the utilization of the NSP-produced dCTP for DNA synthesis more than threefold over baseline values (Fig. 2 B). These findings support previous observations that, under basal conditions, DNA synthesis relies primarily on the DNP-produced dCTP
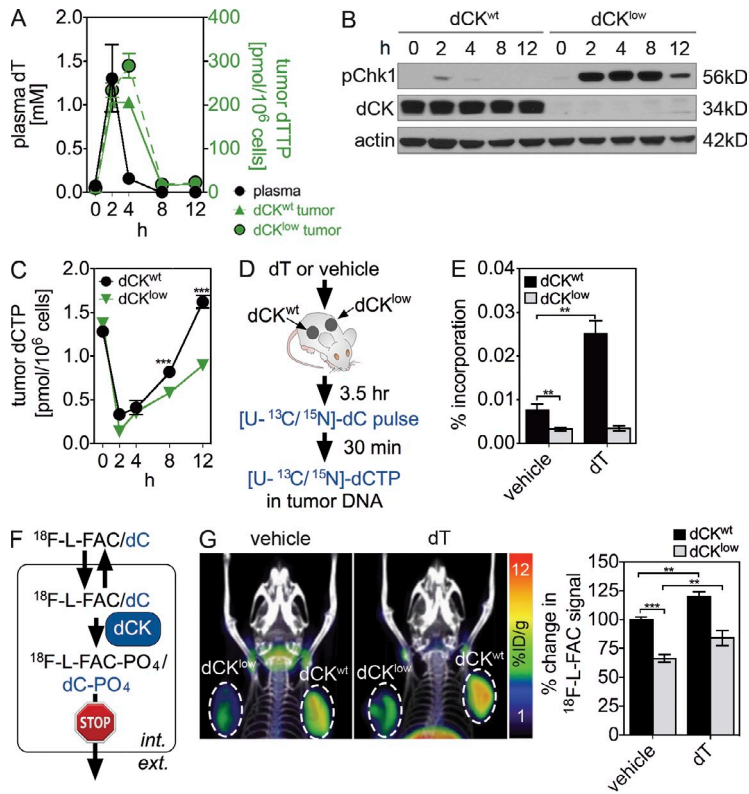
Figure 3. In vivo, salvage of endogenous dC rescues T-ALL cells from RS induced by dT treatment. (A) Left axis: plasma dT levels in NSG mice treated with 2 g/kg dT (single dose). Values are mean ± SEM from $n = 3$ mice/time point; $n = 2$ independent experiments. Right axis: dTTP concentrations from CEM dCK[wt] and dCK[low] tumors at various time points after single-dose dT (2 g/kg) treatment. Values are mean ± SEM, $n = 4$ mice/time point; $n = 2$ independent experiments. (B) Representative immunoblot ($n = 3$ independent experiments) showing pChk1 (Ser345) levels at various time points in bilateral s.c. CEM dCK[wt] and dCK[low] tumors implanted in NSG mice treated with 2 g/kg dT (single-dose). (C) dCTP concentrations from CEM dCK[wt] and dCK[low] tumors at various time points after single-dose dT (2 g/kg) treatment. Values are mean ± SEM, $n = 5$ mice/time point; $n = 2$ independent experiments. ***, $P < 0.001$. (D) Schematic of experimental design for quantifying the incorporation of [U-^{13}C/^{15}N]-dC into the DNA of dCK[wt] and dCK[low] CEM tumors 4 h after single-dose treatment with 2 g/kg dT or vehicle. (E) Quantification of the LC/MS/MS-MRM data for labeled dCTP incorporation into the DNA. Data are mean ± SEM of $n = 6$ mice/group; $n = 2$ independent experiments. **, $P < 0.01$. (F) Schematic of the in vivo PET assay of dCK activity. (G) ^{18}F-L-FAC uptake in s.c. CEM dCK[wt] and dCK[low] tumor xenografts 4 h after vehicle or dT injection. Values represent the mean percent decrease in ^{18}F-FAC signal relative to dCK[wt] vehicle ± SEM, $n = 4$ mice/group; $n = 2$ independent experiments. **, $P < 0.01$; ***, $P < 0.001$.

(Xu et al., 1995). Accordingly, the large size of the NSP-derived free dCTP pool in untreated CEM cells (Fig. 2 B) likely reflects its inefficient utilization for DNA replication under basal conditions. Notably, the NSP-derived free dCTP pool did not decrease in dT-treated cells, even though the utilization of this pool for DNA synthesis increased significantly (Fig. 2 B). This finding suggests that dT up-regulates dCTP production via the NSP, which is consistent with a marked increase in dCK activity (Fig. 2 C) and in dC uptake (Fig. 2 D) in dT-treated CEM cells.

In vivo, salvage of endogenous dC rescues T-ALL cells from RS induced by dT treatment

To examine whether findings from cell culture studies (Figs. 1 and 2) can be recapitulated in vivo, s.c. CEM dCK[wt] and dCK[low] xenografts were established in NOD SCID gamma (NSG) mice. Plasma dT peaked at ∼1.5 mM, 2 h after treatment with a single dT injection (2 g/kg, intraperitoneally) and then rapidly declined to baseline values (∼10 µM) at 8 h (Fig. 3 A). Intratumoral dTTP increased in both dCK[wt] and dCK[low] tumors for at least 4 h after dT administration (Fig. 3 A). In dCK[wt] tumors, dT induced a slight and transient up-regulation of pChk1 at the 2- and 4-h time points (Fig. 3 B). In marked contrast, a more pronounced and sustained pChk1 up-regulation was induced by dT treatment in dCK[low] tumors (Fig. 3 B). These findings suggest that dCK is required to enable CEM cells to resist RS induced by dT treatment in vivo.

To understand the role of dCK in dCTP production and utilization in tumors from dT-treated mice, we measured the free dCTP pool and incorporation of NSP-produced dCTP

into the DNA. During the 0–4-h timeframe, dCTP decreased several-fold in both CEM dCK[wt] and dCK[low] xenografts and then started to recover as plasma dT dropped to baseline values
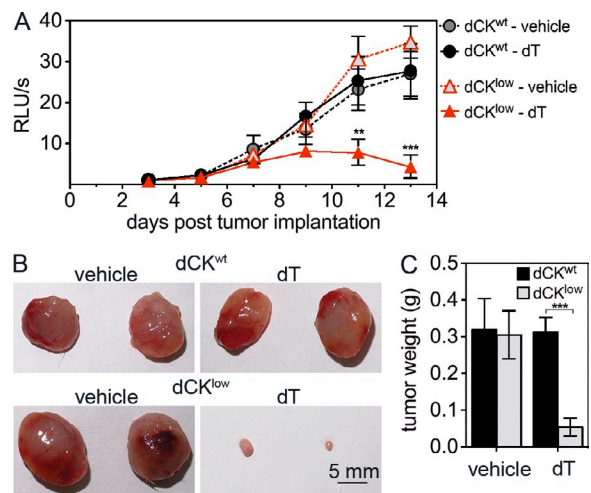

Figure 4. dCK mediates resistance to dT in T-ALL cells in vivo. (A) Serial secreted *Gaussia* luciferase measurements of peripheral blood from NSG mice bearing CEM dCK[wt] or dCK[low] s.c. tumors ($n = 6$ mice/condition) treated every 12 h with vehicle or 2 g/kg dT starting at day 7 after tumor implantation until day 13. Values represent mean ± SEM; $n = 2$ independent experiments. **, $P < 0.01$; ***, $P < 0.001$, compared with dCK[low] vehicle at the indicated time point. (B) CEM dCK[wt] and dCK[low] tumors from vehicle or dT-treated mice from A. (C) Tumor weights (in milligrams) from A. Values represent the mean ± SEM; $n = 2$ independent experiments. ***, $P < 0.001$.
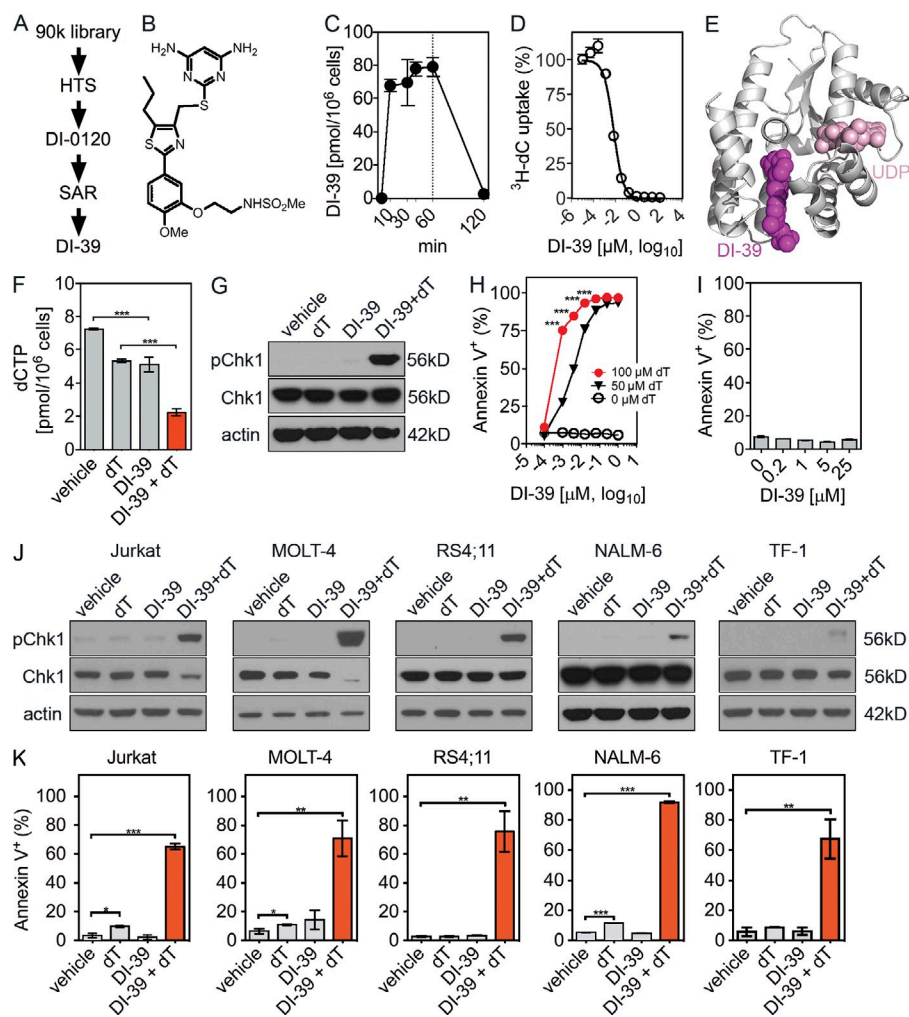
Figure 5. Development of DI-39, a small molecule dCK inhibitor which synergizes with inhibition of de novo dCTP biosynthesis in leukemic cells. (A) Schematic illustrating the development of DI-39, beginning with high-throughput screen (HTS) of a 90,000-compound library, which provided the initial hit DI-0120. Further structural activity relationship (SAR) yielded 80 novel compounds including DI-39. (B) Chemical structure of DI-39. (C) LC/MS/MS-MRM measurements of DI-39 in CEM cells exposed to 1 µM drug for indicated periods of time. Cells were washed three times after 60 min (indicated by vertical line) and cellular drug retention was measured again 60 min later. Values represent mean ± SEM. (D) IC$_{50}$ value of DI-39 determined by percent inhibition of ^{3}H-dC uptake by CEM cells. Values represent mean ± SEM. (E) 2.1 Å crystal structure of dCK with bound DI-39 and uridine diphosphate (UDP). (F) Intracellular dCTP concentrations in cultured CEM dCK^{wt} cells treated with vehicle, 50 µM dT, 1 µM DI-39, or DI-39 + dT for 24 h. Values represent the mean ± SEM; $n = 2$ independent experiments. ***, $P < 0.001$. (G) Representative immunoblots detecting Chk1, pChk1 (Ser345), and actin in CEM cells treated with vehicle, 1 mM dT, 100 nM DI-39, or DI-39 + dT in the presence of 2.5 µM dC for 24 h. (H) Annexin V staining of CEM cells treated for 72 h with indicated concentrations of DI-39 and dT in the presence of 2.5 µM dC. Values are mean ± SEM; $n = 2$ independent experiments. ***, $P < 0.001$ compared with 50 µM dT. (I) Annexin V staining of L1210-10 dCK-null cells treated for 72 h with indicated concentrations of DI-39. Values represent the mean percentage of cells staining positive for Annexin V ± SEM; $n = 2$ independent experiments. (J) Representative immunoblots of Jurkat, MOLT-4, RSR4;11, NALM-6, and TF-1 leukemia cells treated with vehicle, 1 mM dT, 100 nM DI-39, or DI-39 + dT in the presence of 2.5 µM dC for 24 h (NALM-6) or 72 h (Jurkat, MOLT-4, RSR4;11, and TF-1). (K) Annexin V staining of the same panel of leukemia cell lines as in J treated for 72 h with vehicle, 1 mM dT, 100 nM DI-39, or DI-39 + dT. Cultures were supplemented with 2.5 µM dC. Values represent mean percentage of cells staining positive for Annexin V ± SEM; $n = 3$ independent experiments. *, $P < 0.05$; **, $P < 0.01$; ***, $P < 0.001$.

(Fig. 3 C). Notably, intratumoral dCTP recovery occurred significantly slower in the dCK^{low} xenografts than in their wild-type counterparts (Fig. 3 C). To quantify the effects of dT treatment on the utilization of the NSP-produced dCTP for DNA synthesis, tumor-bearing mice were treated with dT or vehicle for 3.5 h and were then pulsed with [U-^{13}C/^{15}N]-labeled dC. 30 min later, mice were sacrificed to measure the incorporation of dCTP produced from labeled dC into tumor DNA by LC/MS/MS-MRM (Fig. 3 D). In tumors from vehicle-treated mice, ∼2-fold less dCTP produced from [U-^{13}C/^{15}N]-labeled dC was incorporated into the DNA of dCK^{low} tumors than in the DNA of their dCK^{wt} counterparts (Fig. 3 E). In dT-treated mice, labeled dCTP incorporation into DNA increased ∼3-fold in dCK^{wt} tumors but remained unchanged in the dCK^{low} xenografts (Fig. 3 E). Together with the pattern of pChk1 up-regulation shown in Fig. 3 B, these findings suggest that upon dT treatment in vivo, dCK activity is required to maintain tumor DNA replication, thereby preventing RS induction. Moreover, similar to in vitro findings (Fig. 2 B), dT treatment in vivo increases the incorporation of NSP-produced dCTP into tumor DNA.

To determine if the increase in the utilization of the NSP-produced dCTP for DNA synthesis in tumors from dT-treated mice is also associated with an up-regulation of the NSP as shown in vitro (Fig. 2, C and D), we took advantage of ^{18}F-L-FAC (1-L-(2′ deoxy-2′,-^{18}Fluoroarabinofuranosyl) cytosine), a fluorinated dC analogue (Radu et al., 2008; Shu et al., 2010). ^{18}F-L-FAC crosses the cell membrane via nucleoside transporters and accumulates specifically in dCK-expressing cells by a phosphorylation-dependent mechanism (Fig. 3 F); dCK-dependent phosphorylated ^{18}F-L-FAC retention in living animals can be imaged and quantified noninvasively by PET. As anticipated, dCK^{low} tumors accumulated ∼40% less ^{18}F-L-FAC than dCK^{wt} tumors (Fig. 3 F). 4 h after dT treatment, ^{18}F-L-FAC accumulation increased by ∼20% in dCK^{wt} tumors (Fig. 3 G). ^{18}F-L-FAC accumulation also increased in
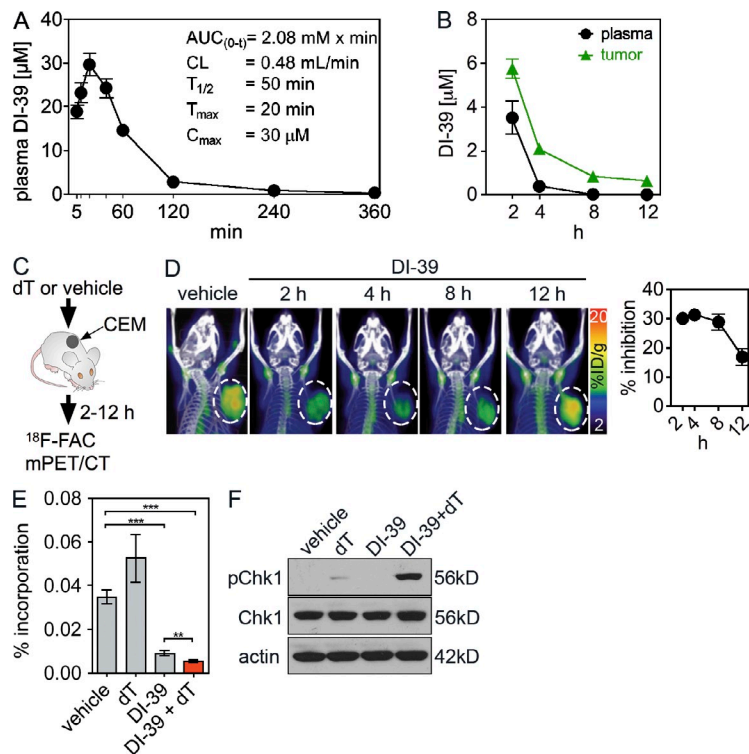
Figure 6. DI–39 inhibits dCK activity in vivo, as determined by ^{18}F–FAC PET, and promotes RS when combined with dT.
(A) Pharmacokinetic profile of DI-39. C57BL/6 mice were dosed with DI-39 via intraperitoneal injection. Dose formulation: 10% DMSO and 40% Captisol (SBE-β-CD, a polyanionic variably substituted sulfobutyl ether of β-cyclodextrin; Stella and He, 2008) in water. Approximated values of the area under the curve (AUC), clearance rate (CL), half-life ($T_{1/2}$), maximum concentration in the plasma (C_{max}), and time to reach the maximum concentration (T_{max}) were calculated using Boomer/Multi-Forte PK Functions for Excel. Values represent the mean ± SD, n = 4/time point; n = 2 independent experiments. (B) LC/MS/MS-MRM quantification of DI-39 concentrations in plasma and CEM tumors at various time points after treatment. See Materials and methods for details. Values represent the mean ± SD, n = 4/group. (C) Schematic illustration of the ^{18}F-FAC PET/CT study to determine in vivo dCK inhibition by DI-39 in CEM s.c. xenografts. (D) Time course of in vivo ^{18}F-FAC PET/CT scans to determine dCK inhibition by DI-39 (single intraperitoneal injection, 50 mg/kg). Values represent the mean percent decrease in ^{18}F-FAC signal ± SD, n = 4 mice/group; n = 2 independent experiments. (E) Percent incorporation of [U-^{13}C/^{15}N]-dC into the DNA of CEM xenografts 5.5 h after single-dose treatment with vehicle, 50 mg/kg DI-39, 2 g/kg dT, or DI-39 + dT. Mice were pulsed with the stable isotope-labeled dC for 30 min before sacrifice. Values represent mean ± SEM, n = 4/group; n = 2 independent experiments. **, $P < 0.01$; ***, $P < 0.001$. (F) Representative immunoblots of pChk1 (Ser345), Chk1, and actin in tumor tissues collected from mice 6 h after treatment with 50 mg/kg DI-39, 2 g/kg dT, or both agents; n = 3 independent experiments.

dCK^{low} tumors (Fig. 3 G), likely because of their residual dCK activity. However, the NSP up–regulation in the dCK^{low} tumors was insufficient to maintain DNA synthesis and prevent RS induction, as indicated by both the marked and sustained pChk1 up–regulation in dCK^{low} tumors from dT-treated mice (Fig. 3 B) and by the low incorporation in dCK^{low} tumors of stable isotope–labeled dCTP into the DNA (Fig. 3 E).

The NSP mediates T–ALL cell resistance to dT treatment in vivo
Because the NSP is required to prevent dT-induced RS in T-ALL cells in culture (Fig. 1 I) and in vivo (Fig. 3 C), we determined if down–regulation of dCK expression synergizes with dT treatment to induce tumor regression in mice. CEM dCK^{wt} and dCK^{low} s.c. tumor-bearing mice were treated with 2 g/kg dT twice daily for 6 d. Prolonged dT administration blocked the growth of CEM dCK^{low} tumors without affecting the dCK^{wt} xenografts, as shown by serial measurements of secreted *Gaussia* luciferase, which served as an indicator of tumor burden in peripheral blood (Tannous, 2009; Fig. 4 A), and end point measurements of tumor sizes (Fig. 4 B) and weights (Fig. 4 C). The synergy between dT treatment and shRNA–mediated dCK down–regulation suggests that pharmacological dCK inhibition, combined with dT administration, may provide a new therapeutic strategy in ALL.

Development of DI–39, a small molecule, high affinity dCK inhibitor that occupies the substrate binding site of the kinase
To examine whether the NSP can be exploited therapeutically through pharmacological dCK inhibition, we screened

selected chemical libraries comprising ∼90,000 small molecules. This high throughput screen (HTS) identified DI-0120 (Fig. 5 A), a dCK inhibitor with an IC$_{50}$ of 1.4 µM in CEM cells. Subsequent structure-activity relationship (SAR) studies yielded DI-39 (Fig. 5 B), a cell-permeable (Fig. 5 C) lead candidate with an IC$_{50}$ of 5 nM, nearly 300-fold lower than that of DI-0120 (Fig. 5 D; Murphy et al., 2013). To investigate how DI-39 inhibits dCK, we obtained a 2.1-Å co-crystal structure, which showed DI-39 occupying the nucleoside-binding site of the kinase and not the nucleotide phosphoryl donor-binding site (Fig. 5 E; Table S1). This mode of binding suggested that DI-39 is a highly specific inhibitor of dCK.

To evaluate DI-39 further, we measured its effects on the dCTP pool of CEM cells. Although treatment with either 1 µM DI-39 or 50 µM dT decreased dCTP by ∼30%, the DI-39/dT combination was synergistic, reducing dCTP in CEM cells by ∼70% (Fig. 5 F). Although in the presence of dC, neither dT nor DI-39 alone induced RS or apoptosis in CEM cells, the DI-39/dT combination triggered both RS, as measured by pChk1 up-regulation (Fig. 5 G), and apoptosis, as measured by Annexin V staining (Fig. 5 H). Notably, when the dCK-null leukemia cell line L1210-10K (Jordheim et al., 2004) was treated with increasing concentrations of DI-39 far above those required to inhibit dCK activity or to kill CEM cells when combined with dT, it did not induce apoptosis, further supporting the selectivity of DI-39 for dCK (Fig. 5 I). The DI-39/dT combination also induced RS (Fig. 5 J) and apoptosis (Fig. 5 K) in four other ALL cell lines (Jurkat, MOLT-4,
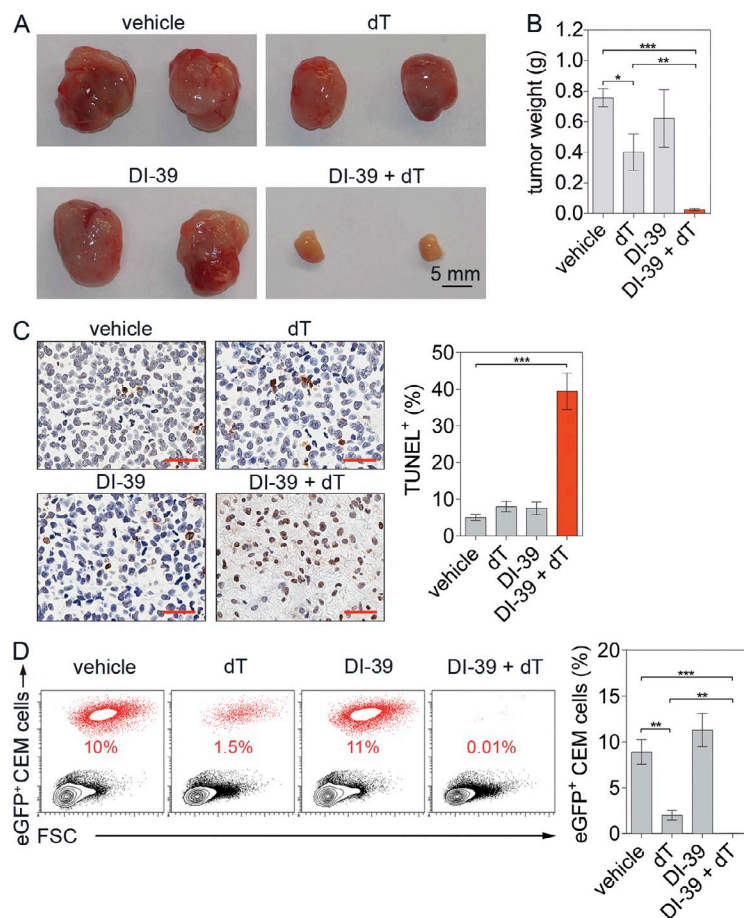
Figure 7. Pharmacological co-targeting of DNP and NSP dCTP production is effective against T-ALL cells in vivo. (A) Representative images of CEM xenografts isolated from mice treated with vehicle, 2 g/kg dT, 50 mg/kg DI-39, or DI-39 + dT every 12 h beginning at day 7 after inoculation and continuing to day 14. $n = 6$ mice/group; $n = 2$ independent experiments. (B) Tumor weights from A. Values represent mean ± SEM; $n = 2$ independent experiments, $n = 6$ mice/group. *, $P < 0.05$; **, $P < 0.01$; ***, $P < 0.001$. (C) Representative images and quantification of TUNEL staining of tumor samples from A. Bars, 50 μm. Values represent mean ± SEM, $n = 6$ mice/group. ***, $P < 0.001$. (D) Representative FACS plots and quantification of eGFP + CEM leukemia cells in the BM of NSG mice treated with vehicle, 2 g/kg dT, 50 mg/kg DI-39, or DI-39 + dT. Mice ($n = 6$/group) were treated every 12 h beginning at day 3 after inoculation with 1.0×10^6 CEM cells. Values represent mean ± SEM; $n = 2$ independent experiments. **, $P < 0.01$; ***, $P < 0.001$.

RS4;11, and NALM-6) as well as in an erythroleukemia cell line (TF-1). In summary, DI-39 enters cells, inhibits the NSP-dependent dCTP production, and synergizes with dT to induce lethal RS in multiple leukemia cell lines.

DI-39 inhibits tumor dCK activity in vivo and promotes RS when combined with dT

To evaluate DI-39 in vivo, we determined its pharmacokinetics (PK) in plasma and in tumor tissues. The plasma half-life of DI-39 was ~50 min (Fig. 6 A), and detectable amounts of drug (~15 nM) were present in tumor tissues 8 h after single dose administration (Fig. 6 B). To correlate the amount of DI-39 in plasma and tumor at 2, 4, 8, and 12 h after administration of the drug with the pharmacodynamic (PD) effect of DI-39 (i.e., inhibition of tumor dCK activity), we performed ^{18}F-FAC PET/CT scans of CEM tumor-bearing mice at these time points (Fig. 6 C). DI-39 (50 mg/kg, administered intraperitoneally) reduced ^{18}F-FAC accumulation in tumors by ~30% for up to 8 h (Fig. 6 D). This level of reduction was comparable with that obtained in the dCK knockdown model (Fig. 3 E). The timing of recovery of tumor dCK activity, determined with PET, after DI-39 administration, indicates that sustained target inhibition could be obtained by administering DI-39 every 12 h. Notably, this information could not be obtained from conventional plasma PK measurements (Fig. 6 A).

To further investigate the effects of DI-39 on tumor dCTP metabolism, 5.5 h after treatment with dT and/or DI-39, CEM tumor-bearing mice were pulsed for 30 min with [U-^{13}C/^{15}N]-dC. LC/MS/MS-MRM was used to quantify label incorporation into DNA. Analogous to our dCK knockdown results (Fig. 3 F), DI-39 significantly reduced [U-^{13}C/^{15}N]-dC incorporation into the DNA of CEM cells (Fig. 6 E). Moreover, the DI-39/dT combination promoted RS in CEM tumors, as indicated by pChk1 up-regulation (Fig. 6 F). Together, these findings indicate that DI-39 efficiently inhibits tumor dCK activity in vivo for up to 12 h, the DI-39/dT combination induces RS in CEM cells in vivo, and PET imaging provides a useful PD companion biomarker for DI-39.

Pharmacological co-targeting of DNP and NSP dCTP biosynthesis with DI-39 and dT blocks the growth of T-ALL xenografts in mice

The therapeutic efficacy of the DI-39/dT combination was first tested in mice bearing established s.c. CEM xenografts. Only the combination therapy dramatically reduced tumor burden in these mice, as indicated by end point tumor sizes (Fig. 7 A) and weights (Fig. 7 B). In addition, TUNEL staining from harvested tumors indicated significant induction of DNA breaks only with the DI-39/dT combination (Fig. 7 C). In contrast to findings shown in Fig. 4, dT treatment alone
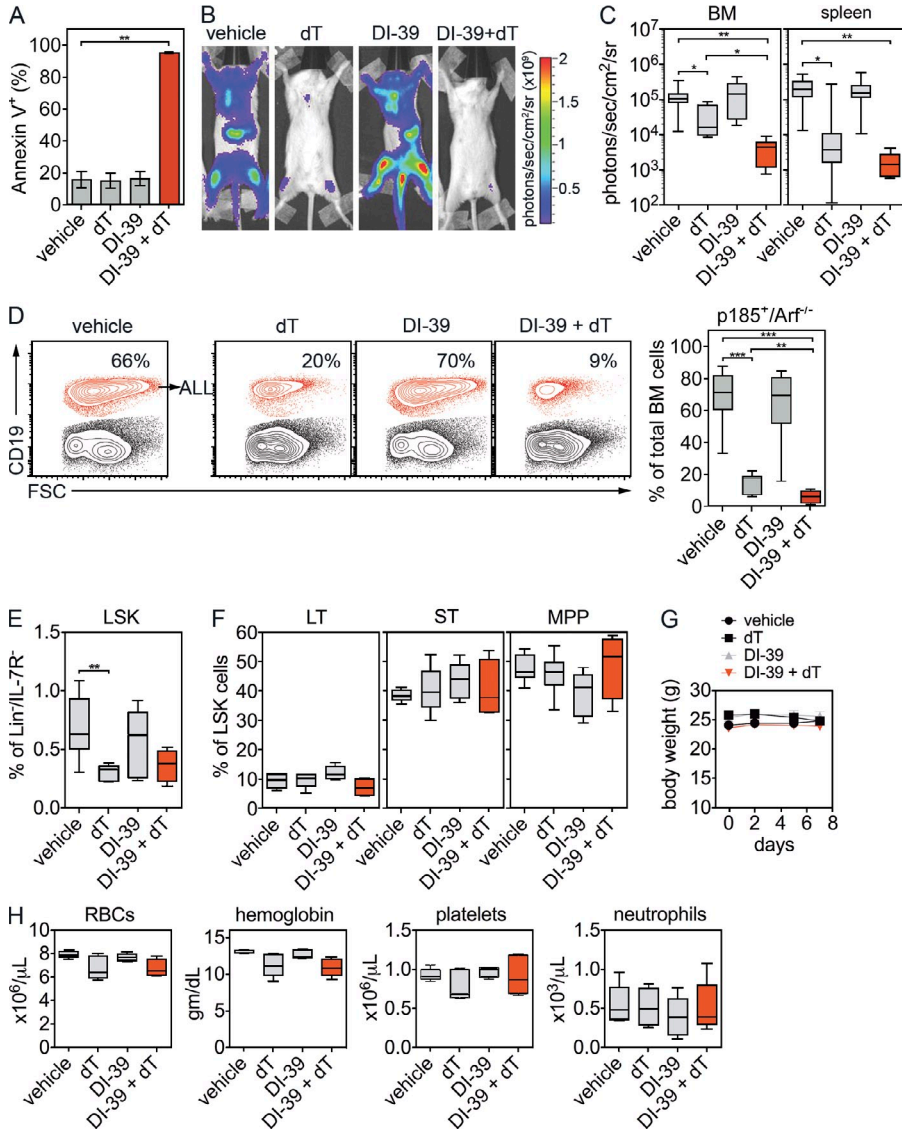
Figure 8. Pharmacological co-targeting of the DNP and NSP is efficacious against primary mouse p185^BCR-ABL *Arf*^−/− Pre–B ALL cells, while sparing the hematopoietic progenitor pool. (A) Annexin V staining of p185^BCR-ABL *Arf*^−/− pre–B cells after 48-h treatment with vehicle, 200 µM dT, 100 nM DI-39, or DI-39 + dT in the presence of 2.5 µM dC. Values are mean ± SEM; n = 2 independent experiments. **, P < 0.01. (B) Representative BLIs of mice (n = 6/group) treated with vehicle, 2 g/kg dT, 50 mg/kg DI-39, or DI-39 + dT at day 14 after intravenous injection of 2.0×10^4 pre–B leukemia cells/mouse. (C) Quantification of BLI from in BM and spleen. *, P < 0.05; **, P < 0.01. (D) Representative FACS analyses and quantification of CD19+ leukemic cells in the BM of treated mice. **, P < 0.01; ***, P < 0.001. (E) Quantification of Lineage− Sca-1+ c-Kit+ (LSK) populations from treated mice. **, P < 0.01. (F) LSK cells from BM of treated mice were analyzed for expression of CD34 and Flt3 to identify and quantify long-term (LT, CD34−, Flt3−), short-term (ST, CD34+, Flt3−), and multipotent progenitor (MPP, CD34+, Flt3+) stem cells. (G and H) Body weights (G), as well as RBC, hemoglobin, platelet, and neutrophil measurements (H) of NSG mice (n = 6/group) treated with vehicle, 2 g/kg dT, 50 mg/kg DI-39, or DI-39 + dT every 12 h for 7 d. Data represent mean ± SEM. All data are representative of at least two independent experiments.

had a small but significant effect on the size and weight of CEM tumors (Fig. 7, A and B). This difference is likely explained by a slight increase in dT PK by the Captisol/DMSO formulation used to co-administer DI-39 with dT; DI-39 has limited solubility in aqueous saline solutions. The therapeutic efficacy of the DI-39/dT combination was further confirmed in a systemic T-ALL model, in which CEM cells were injected intravenously. In the systemic T-ALL model, treatment with dT alone induced an ∼7-fold reduction in the percentage of leukemic cells in BM relative to vehicle and DI-39–treated groups (Fig. 7 D). This finding suggests that BM-resident leukemic cells are more susceptible to dT in vivo than they are in cell culture. However, the DI-39/dT combination reduced tumor burden by an additional 100-fold relative to dT alone, indicating strong synergy between these two therapeutic agents (Fig. 7 D). Therefore, pharmacological co-targeting of both the DNP and NSP dCTP biosynthetic pathways is highly effective against CEM leukemic cells in vivo.

The combination therapy is effective against a primary B-ALL systemic model and has minimal effects on the normal hematopoietic progenitor pool

We next assessed the efficacy of the DI-39/dT combination therapy against short-term cultures of murine BCR-ABL (p185), Arf^−/− pre–B ALL cells (p185^BCR-ABL/Arf^−/−; Williams et al., 2006; Boulos et al., 2011). Although primary B-ALL cells were sensitive in culture to the DI-39/dT combination, they required fourfold more dT than the CEM T-ALL cell line for optimal induction of apoptosis (Fig. 8 A). This finding is consistent with previous clinical observations that B-ALL cells are less sensitive to dT treatment than T-ALL cells (Kufe et al., 1980). To evaluate the efficacy of dT and/or DI-39 in an in vivo B-ALL model, firefly luciferase–marked p185^BCR-ABL/Arf^−/− cells were inoculated intravenously in NSG mice. 11 d after inoculation, bioluminescence imaging (BLI) of firefly luciferase–marked p185^BCR-ABL/Arf^−/− ALL-bearing NSG mice treated with vehicle or 50 mg/kg DI-39 revealed substantial
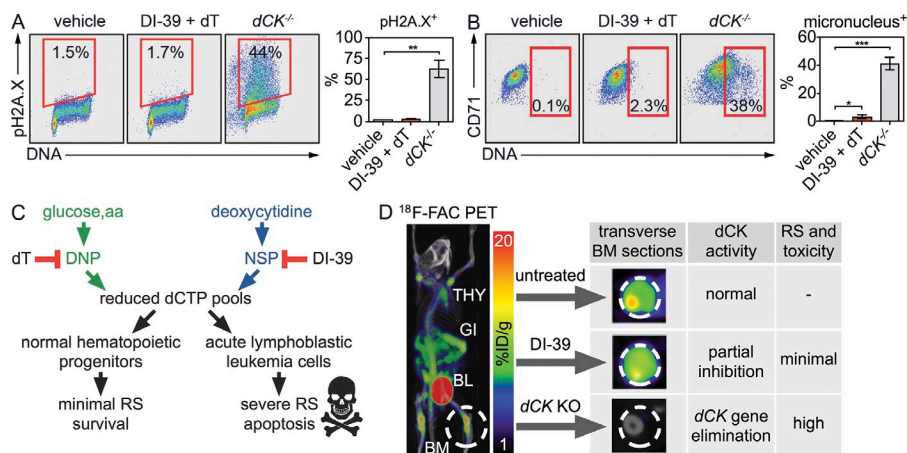
Figure 9. Assessment of potential toxicity of the DI–39/dT combination therapy and model. (A) Representative FACS staining of pH2A.X and data quantification in EryA (CD71+/high forward scatter) erythroblasts to estimate endogenous (for $dCK^{-/-}$ mice, $n = 4$ mice/group) or potential pharmacologically induced (DI-39 + dT) genotoxic stress. NSG mice ($n = 5$ mice/group) were treated with vehicle or combination of 50 mg/kg DI-39 and 2 g/kg dT every 12 h for 8 d. Values are mean ± SEM. **, $P < 0.01$. (B) Representative FACS plots and quantification of micronucleated erythrocytes indicative of endogenous (for $dCK^{-/-}$ mice) or potential pharmacologically induced (DI-39 + dT) genotoxic stress. Values represent mean ± SEM from $n = 2$ independent experiments. *, $P < 0.05$; ***, $P < 0.001$. (C and D) Proposed rationale for explaining the selectivity of the combination therapy for leukemia cells relative to normal hematopoietic progenitors (see text for details).

systemic disease with focal BM and spleen localization (Fig. 8 B). Although dT (2 g/kg) treatment significantly reduced BLI signals in BM and spleen, the addition of DI-39 had a more pronounced effect than dT alone (Fig. 8, B and C). To confirm the BLI findings, we also analyzed the leukemia burden in BM by flow cytometry using CD19 (a B cell marker which, in NSG mice, is present only on the leukemia cells; Fig. 8 D). Treatment with dT induced a significant decrease in the percentage of p185[BCR-ABL]/Arf^{−/−} ALL cells relative to vehicle-treated mice (Fig. 8 D). The addition of DI-39 resulted in an additional ∼2-fold reduction in the percentage of leukemic cells compared with dT alone (Fig. 8 D). These findings, using primary p185[BCR-ABL]/Arf^{−/−} cells, indicate that the DI-39/dT combination is effective against an aggressive in vivo B-ALL model.

In parallel with analyses of BM-resident leukemic cells, we also assessed the effects of the combination therapy on the hematopoietic progenitor pool. We analyzed the Lineage− Sca-1+ c-Kit+ (LSK) HSC population, as well as short-term (ST), long-term (LT), and multipotent progenitor (MPP) hematopoietic progenitor cells. With the exception of a minor decrease in the percentage of LSK upon dT treatment (Fig. 8 E), there were no significant changes between control and treated groups (Fig. 8, E and F; and Fig. S1, A and B). Therefore, the combination therapy preferentially targets BM-resident leukemia cells while sparing normal hematopoietic progenitors. In addition, DI-39 alone or in combination with dT, when administered twice a day for 7 d in NSG mice, did not affect body weight (Fig. 8 G) and had no detectable effects on RBCs, hemoglobin, platelets, or neutrophils (Fig. 8 H).

Partial inhibition of dCK in hematopoietic tissues prevents hematological toxicity from dT and DI-39

To further investigate the potential hematological toxicity of the combination therapy, we took advantage of our $dCK^{-/-}$ mice (Austin et al., 2012). This approach allowed us to directly compare the effects on the hematopoietic system induced by complete loss of dCK function in the $dCK^{-/-}$ mice with the effects induced pharmacologically in dCK wild-type mice ($dCK^{+/+}$) by DI-39 and dT. In the erythroid lineage, the DI-39/dT combination induced markedly less DNA damage and genotoxicity in the $dCK^{+/+}$ mice, as measured by pH2A.X staining (Fig. 9 A) and the micronucleus assay, respectively (Fig. 9 B), than did dCK gene elimination alone in $dCK^{-/-}$ mice. These findings indicate that pharmacological inhibition of dCK activity by DI-39, alone or in combination with dT treatment, is better tolerated than complete elimination of dCK enzymatic activity by genetic dCK gene inactivation.

DISCUSSION

We demonstrate here a requirement for a functional NSP in T-ALL and B-ALL cells to prevent dCTP pool insufficiency, RS, and apoptosis after pharmacological inhibition of de novo dCTP synthesis. We introduce DI-39, a new small molecule inhibitor of dCK; dCK is the kinase required for the compensatory metabolic switch, triggered by dT-mediated DNP inhibition, to NSP-dependent dCTP biosynthesis. We elucidate how DI-39 inhibits dCK by obtaining a high-resolution crystal structure of the inhibitor–dCK complex. We demonstrate the therapeutic efficacy of co-targeting both the DNP and NSP dCTP biosynthetic pathways, using in vivo models of T-ALL and B-ALL, without detectable toxicity against normal hematopoietic progenitors. We also describe a companion pharmacodynamic PET assay of dCK enzyme activity, which allows noninvasive in vivo imaging of pharmacological interventions targeting dCTP biosynthesis.

Selectivity of the DI–39/dT combination therapy for leukemic cells relative to normal hematopoietic progenitors

Our current working model to explain the mechanism and observed selectivity of the combination therapy for leukemia

cells relative to normal hematopoietic progenitors is depicted schematically in Fig. 9 (C and D). According to this model, pharmacological co-targeting of the DNP (by dT) and of the NSP (by DI-39) is highly effective at inducing lethal RS against T- and B-ALL cells and has minimal effects on normal hematopoietic cells. As indicated by ^{18}F-FAC PET imaging of dCK activity (Fig. 6 D and Fig. 9 D), DI-39 induced partial inhibition of dCK in normal BM cells compared with the complete loss of dCK activity in $dCK^{-/-}$ mice (Toy et al., 2010; Austin et al., 2012). The residual dCK activity in BM cells after DI-39 treatment may be sufficient to prevent the more substantial reductions observed for the dCTP pools of hematopoietic progenitors in the $dCK^{-/-}$ mice. This model of low or absent toxicity due to partial inhibition of the therapeutic target is reminiscent of recent work in which hypomorphic ATR suppression was lethal to tumor tissues exposed to oncogenic stress yet had only minimal toxicity to normal tissues (Bartek et al., 2012; Schoppy et al., 2012). Furthermore, the enhanced susceptibility of ALL cells to a reduced supply of dCTP could reflect the inherent inability of these leukemic cells to mount an efficient RS response. Although additional studies are required to precisely identify the defects in cell cycle checkpoints that increase the susceptibility of ALL cells to RS induced by dNTP insufficiency, when compared with normal hematopoietic progenitor cells, we note the presence of inactivating *TP53* mutations in several tested ALL cell lines. In this context, it has been suggested that, in normal cells with wild-type p53, the skewing in dNTP pools induced by inhibition of de novo pyrimidine synthesis by PALA (*N*-(phosphonacetyl)-ʟ-aspartate) creates reversible DNA damage that is sufficient to activate p53 and induce the expression of proteins that provide protective arrest at multiple cell cycle checkpoints (Hastak et al., 2008). In cancer cells with defects in p53 or in its downstream effectors, failure to arrest DNA synthesis when pyrimidine dNTP pools are depleted leads to irreversible DNA damage that eventually causes apoptosis (Hastak et al., 2008).

Potential clinical implications

High avidity for dT has been previously identified as a potential metabolic liability of certain cancers, leading to clinical studies using high dT doses as a potential therapeutic (O'Dwyer et al., 1987). Prolonged (over 5 d) dT infusions have shown responses in heavily pretreated T-ALL and cutaneous T cell lymphoma patients, with the side effects encountered being tolerable, manageable, and reversible (Chiuten et al., 1980; Kufe et al., 1980, 1981). However, therapeutic responses to dT in these patients were, in general, limited and transient, potentially reflecting the ability of the NSP, via dCK, to compensate for the dCTP-depleting effect of dT. Because potent small molecule inhibitors of dCK have recently been described (Yu et al., 2010; Murphy et al., 2013), future clinical studies can determine if the anti-leukemic activity of dT reported in T-ALL and cutaneous T cell-lymphoma patients can be significantly improved by pharmacological blockade of the dC salvage pathway.

Companion diagnostics for therapies targeting dCTP biosynthetic pathways in cancer

The data presented here provide examples of both in vivo and in vitro companion diagnostics (or biomarkers) that could assist the clinical translation of the DI-39/dT combination therapy. For example, direct assessments of temporal changes in tumor dCK activity in vivo with PET were more useful than conventional plasma pharmacokinetic measurements for identifying the optimal schedule for the DI-39/dT combination therapy (Fig. 6). Because our PET assays for monitoring dCK activity have already been translated to humans (Schwarzenberg et al., 2011), approaches similar to those described in our preclinical experiments could be used in future clinical trials to noninvasively monitor dCK inhibition in target tissues in vivo. Up-regulation of pChk1 and pH2A.X levels by leukemia cells upon DI-39/dT treatment (Fig. 6 F) could provide additional pharmacodynamic biomarkers of DNA damage, as shown previously for PARP inhibitors (Fong et al., 2009). Furthermore, because the efficacy of the DI-39/dT therapy depends on the capacity of tumors cells to take up large amounts of dT and convert it to dTTP, PET imaging using ^{18}F-FLT (3′-deoxy-3′-fluorothymidine), a probe for dT metabolism (Shields et al., 1998), may enable the identification of tumors with unusually high avidity for dT. Thus, ^{18}F-FLT PET may match the proposed definition of a predictive or enrichment biomarker (de Bono and Ashworth, 2010) for dT-based therapies.

Regulation of the NSP by the DNA damage response (DDR) pathway

Our in vitro (Fig. 2 C) and in vivo (Fig. 3, E and F) data indicate that, in CEM T-ALL cells, dT treatment up-regulated the activity of the NSP. Although NSP up-regulation by dT treatment may result from a decrease in the negative feedback by dCTP on dCK activity (Datta et al., 1989), additional mechanisms could also be involved. For example, dCK activity is increased by treatment with DNA damaging agents that do not affect dCTP production via the DNP (Ooi et al., 1996; Csapo et al., 2003). Moreover, dCK activation after DNA damage involves phosphorylation of the kinase on serine 74 (Yang et al., 2012). This serine is part of an SQ/TQ motif, which is a typical phosphorylation site for ATM and ATR kinases in the DDR pathway. Indeed, dCK has been identified as a direct target of these kinases (Matsuoka et al., 2007). Therefore, after DNA damage induced by high dose dT and, potentially, by other genotoxic therapies, the DDR pathway may promote NSP up-regulation via posttranslational regulation of dCK to expand dNTP pools and facilitate DNA repair. If correct, this model provides a rationale for testing dCK inhibitors in combination with radiation therapy and other genotoxic therapies.

In summary, our results provide new insight into the nucleotide metabolism of leukemic cells and also demonstrate a new therapeutic strategy to overcome the redundancy and adaptability of nucleotide metabolism in ALL and, possibly, in other hematological malignancies in which uncontrolled expansion of the dTTP pool by dT treatment results in a potential metabolic liability. Similar approaches that fit within the

conceptual framework of targeting non–oncogene addiction (Luo et al., 2009) may be applicable to other redundant biosynthetic pathways that provide survival advantages to tumor cells.

MATERIALS AND METHODS

Cell lines and culture conditions. Human cell lines CCRF-CEM, Jurkat, MOLT-4, RSR4;11, and TF-1 were obtained from American Type Culture Collection. NALM-6 and L1210-10K cells were a gift from M. Teitell (UCLA) and C. Dumontet (Université Claude Bernard Lyon I, Lyon, France), respectively. All cell lines were maintained in 5% FBS in RPMI-1640 and were grown at 37°C, 20% O_2, and 5% CO_2.

Animals. Mice were bred and housed under specific pathogen-free conditions and were treated in accordance with the UCLA Animal Research Committee protocol guidelines. The $dCK^{-/-}$ were generated and bred as previously described and backcrossed to C57BL/6 mice for $n = 7$ generations (Toy et al., 2010; Austin et al., 2012). Age-matched (5–12 wk old) WT and $dCK^{-/-}$ littermates were used to assess RS induction by dT in BM myeloid cells.

Reagents, antibodies, immunoblotting, and flow cytometry. dT, 2′-dC, hydroxyurea, 5-FU, and cisplatin (all Sigma-Aldrich) were prepared in DMSO or water. Lentiviral shRNA constructs against dCK and nontargeting control were from Sigma-Aldrich. For cell culture assays, dCK inhibitors were resuspended in DMSO. Immunoblotting was performed as previously described (Austin et al., 2012). The following antibodies and reagents for immunoblotting were purchased: phospho-Chk1 Ser345, phospho-Chk2 Thr68, Chk1, Chk2, anti–mouse HRP-conjugated IgG, and anti–rabbit HRP-conjugated IgG (Cell Signaling Technology); dCK and β-actin (Sigma-Aldrich); and TK1 (Abcam). Bound antibody was detected using chemiluminescence immunoblotting detection reagents (Thermo Fisher Scientific). Isolation and FACS phenotyping of hematopoietic stem cells, EryA, and myeloid was performed as previously described (Austin et al., 2012). The p185$^{BCR-ABL}$/Arf$^{-/-}$ cells were identified using an anti-CD19 (APC) antibody. For cell cycle analyses, total DNA content was determined using 1 µg/ml DAPI or 20 µg/ml propidium iodide containing 5 µg/ml RNase A. Annexin V staining was performed according to the manufacturer's protocol (BD). For the micronucleus assay, isolated BM cells were stained with the following antibodies (eBioscience): Ter119 PerCP-Cy5.5 (TER-119), CD71 APC (R17217), CD45 PE-Cy7 (30-F11), CD61 PE (2C9.G3), and CD11b APC-eFluor780 (M1/70). Cells were stained, washed, and fixed with Cytofix/Cytoperm solution (BD). Cells were then washed and stained with 1 µg/ml DAPI in PBS/2% FBS. All flow cytometry data were acquired on a four-laser LSRII cytometer (BD) and analyzed using FlowJo (Tree Star).

Measurements of dT and DI-39 pharmacokinetics in mice. NOD SCID gamma (NSG) mice were injected with 2 g/kg dT intraperitoneally. 75 µl of whole blood was obtained at 0, 2, 4, and 8 h through retro-orbital sinus bleed using hematocrit capillary tubes. Whole blood was immediately centrifuged at 3,000 g for 5 min to isolate serum. 30 µl of serum was mixed with 1 ml methanol/acetonitrile (1:9), vortexed for 2 min, and centrifuged at 14,000 g for 4 min at 4°C. Extraction was repeated and the pooled supernatant was dried under vacuum centrifugation. The residue was dissolved in 100 µl water, filtered, and eluted through a microBondapak C18 column (Waters) under a gradient mobile phase from 2 to 50% methanol over 10 min at a flow rate of 1.5 ml/min. dT was detected by absorbance intensity (254 nm), and concentrations were interpolated from standard curves.

To determine the pharmacokinetic profile of DI-39, C57BL/6 female mice were dosed with DI-39 via intraperitoneal injection according to a previously described protocol (Murphy et al., 2013). Dose formulations include 10% DMSO and 40% Captisol (SBE-β-CD, a polyanionic variably substituted sulfobutyl ether of β-cyclodextrin; Stella and He, 2008) in water. Approximately 75 µl of whole blood was obtained at various time points starting at 5–360 min through retro-orbital sinus bleed using hematocrit capillary tubes. Approximated values of the area under the curve (AUC),

clearance rate (CL), half-life ($T_{1/2}$), maximum concentration in the plasma (C_{max}), and time to reach the maximum concentration (T_{max}) were calculated using Boomer/Multi-Forte PK Functions from Excel (Microsoft).

For the DI-39 tumoral and plasma uptake study using LC/MS/MS-MRM, tumor-bearing NSG mice were injected with 50 mg/kg DI-39 intraperitoneally at 0, 2, 4, 8, and 12 h before sacrifice. Whole tumors were excised, weighed, and homogenized with an equal volume of 2-mm-diameter stainless steel beads (Next Advance) in 1 ml of ice-cold acetonitrile/water (50/50, vol/vol) containing 0.5 pmol/µl of the internal standard DI-70 (2-(((2-(4-methoxy-3-(2-(2-(2-methoxyethoxy)ethoxy)ethoxy)phenyl)-5-propylthiazol-4-yl)methyl)thio)pyrimidine-4,6-diamine, $C_{25}H_{35}N_5O_5S_2$, molecular mass = 549.2 g/mol, an in-house synthesized DI-39 analogue) in a Bullet Blender homogenizer (Next Advance). Tissue homogenates were left overnight at 4°C on a shaker and the next day centrifuged at 20,000 g for 10 min. 700 µl of the supernatant was transferred to a clean tube and was evaporated to dryness in a vacuum centrifuge. The residue was reconstituted in 100 µl acetonitrile/water (50/50, vol/vol). For plasma measurements, ∼100 µl of blood was collected through a retro-orbital sinus bleed using capillary blood collection tubes. Samples were centrifuged at 20,000 g for 5 min, and 30 µl of the supernatant was transferred into a clean tube. The sample was mixed with 500 µl ice-cold acetonitrile/water (50/50, vol/vol) containing the internal standard and processed in the same way as the tumor homogenates. Calibration standards were prepared by spiking working stock solution of DI-39 in tumor homogenates and plasma from untreated mice to give the following range: 0.02–20 pmol/µl. 5-µl samples were injected onto a reverse phase column (ZORBAX Rapid Resolution High Definition [RRHD] Eclipse Plus C18 [Agilent Technologies], 2.1 × 50 mm, 1.8 µm) equilibrated in water/acetonitrile/formic acid, 95/5/0.1, and eluted (200 µl/min) with an increasing concentration of solvent B (acetonitrile/formic acid, 100/0.1, vol/vol: min/% acetonitrile; 0/5, 0/5, 2/5, 8/80, 9/80, 10/5, and 12/5). The effluent from the column was directed to an electrospray ion source (Jet Stream; Agilent Technologies) connected to a triple quadrupole mass spectrometer (6460 QQQ; Agilent Technologies) operating in the positive ion MRM mode. The ion transitions for DI-39 and DI-70 (525.2→383.3 and 550.2→408.2, respectively) were recorded under previously optimized conditions. The DI-39 peak areas were normalized to the internal standard and tumor weight.

The experiment using CCRF-CEM cells to measure the uptake of DI-39 in cell culture followed a similar protocol as the one described above. CCRF-CEM cells were cultured in 5% FBS in RPMI-1640 media supplemented with 1 µM DI-39 for 10, 30, 40, and 60 min before cell extraction. For some samples, the media with 1 µM DI-39 was removed and the cells were washed three times in PBS before adding fresh media without DI-39 for 60 min. The cells were extracted and homogenized in 1 ml ice-cold acetonitrile/water (50/50, vol/vol) containing 0.5 pmol/µl of the same internal standard as mentioned before. The cell extract was left overnight at 4°C on a shaker and the next day centrifuged at 20,000 g for 10 min. The supernatant was transferred to a clean tube and was evaporated to dryness in a vacuum centrifuge. The residue was reconstituted in 100 µl acetonitrile/water (50/50, vol/vol). DI-39 was quantified as described above.

Incorporation of stable isotope–labeled glucose and dC into the free dCTP pool and into DNA. CEM cells were transferred into RPMI supplemented with 5% dialyzed FCS containing 10 µM uniformly labeled [U-^{13}C/^{15}N]-dC (Cambridge Isotopes), 2 g/liter of uniformly labeled [U-^{13}C]-glucose (Cambridge Isotopes), and 0, 50, or 250 µM dT. For the dNTP analysis, the cells were extracted overnight at −20°C with 75% methanol. The extracts were then heated in boiling water for 3 min, pelleted, and the supernatants were transferred and dried under vacuum centrifugation. For DNA analysis, cells were collected and genomic DNA was extracted using the Quick-gDNA MiniPrep kit (Zymo Research). Genomic DNA was then digested to nucleosides using the DNA Degradase Plus kit (Zymo Research).

For the in vivo studies, tumor-bearing mice were injected with 200 µl of 2.5 mM [U-^{13}C/^{15}N]-dC 30 min before sacrifice. Tumors were harvested, mechanically digested into single cells, and cell counts were obtained. DNA extraction was performed as described above.

DNA hydrolysis samples were diluted 1/1 with solvent A (water/formic acid, 100/0.2, vol/vol) and analyzed using a modified version of a previously reported method (Cohen et al., 2009) in which 10-µl aliquots of the solution were injected onto a porous graphitic carbon column (Thermo Hypercarb, 100 × 2.1 mm, 3-µm particle size) equilibrated in solvent A and eluted (300 µl/min) with an increasing concentration of solvent B (acetonitrile/min/% B; 0/0, 6/60, 6.1/100, 9/100, 9.1/0, and 10/0). The effluent from the column was directed to Jet Stream–connected 6460 QQQ (Agilent Technologies) operating in the positive ion MRM mode. After verification of retention times using authentic standards, the peak areas of the MH^+→fragment ion transitions for the dC isotopomers (M_0, 228.1→112.1; M_1, 229.1→112.1; M_2, 230.1→112.1; M_3, 231.1→112.1; M_4, 232.1→112.1; M_5, 233.1→112.1; M_6, 234.1→113.1; M_7, 235.1→114.1; M_8, 236.1→115.1; M_9, 237.1→116.1; M_{10}, 238.1→117.1; M_{11}, 239.1→118.1; and M_{12}, 240.1→119.1) were recorded with instrument manufacturer-supplied software (MassHunter; Agilent Technologies) and normalized to cell number. The dC isotopomers of M_3 through M_8 for the DNP and M_{11} through M_{12} for NSP were detected and used for data analysis.

For free dNTP analysis, a modified version of the same previously reported method (Cohen et al., 2009) was used in which dried samples were redissolved in 100 µl solvent C (5 mM hexylamine and 0.5% mM diethylamine, pH 10.0) and 10-µl aliquots were injected onto porous graphitic carbon column (Hypercarb, 150 × 2.1 mm, 3-µm particle size; Thermo Fisher Scientific) equilibrated in solvent C and eluted (150 µl/min) with an increasing concentration of solvent D (acetonitrile/min/% D; 0/0, 5/0, 25/40, 25.1/100, 30/100, 30.1/0, and 40/0). The effluent from the column was directed to the same instrument described above, operating in the negative ion mode. After verification of retention times using authentic standards, the intensities of preselected $(M–H)^-$→fragment ion transitions for various dCTP isotopomers (M_0, 466.0→159.0; M_1, 467.0→159.0; M_2, 468.0→159.0; M_3, 469.0→159.0; M_4, 470.0→159.0; M_5, 471.0→159.0; M_6, 472.0→159.0; M_7, 473.0→159.0; M_8, 474.0→159.0; M_9, 475.0→159.0; M_{10}, 476.0→159.0; M_{11}, 477.0→159.0; and M_{12}, 478.0→159.0) were recorded, again with instrument manufacturer-supplied software (MassHunter), and normalized to cell number. The dCTP isotopomers of M_5 through M_8 for the DNP and M_{12} for NSP were detected and used for data analysis. The M_3 and M_4 isotopomers were not detected.

dNTP pool measurements. Intracellular dNTP pool measurements were conducted as previously described (Austin et al., 2012).

Comet assay. The comet assay was performed according to the CometAssay reagent kit protocol (Trevigen) under alkaline conditions. For quantification, four random sections of each slide containing >100 cells were imaged and Olive Tail Moment obtained using Cometscore (TriTek) software.

Generation of luciferase viral construct, and retroviral gene transduction. The gene encoding humanized secreted *Gaussia* luciferase (sGluc), pCMV-GLuc-1 (Nanolight Technology), was subcloned into the MSCV-IRES-GFP retroviral vector. Pheonix-Ampho cells were transfected with the generated vector using Lipofectamine transfection reagent (Invitrogen). 48 h after transfection, virus was harvested and used to transduce CEM dCK[wt] and CEM dCK^{low} cells. GFP-positive cells were sorted with a FACSAria II cell sorter (BD).

Crystallization of DI-39 in complex with dCK and UDP. The C4S S74E dCK variant used for crystallographic studies was expressed and purified as described in Nomme et al. (2014). Crystallization, x-ray data collection, and refinement were also performed as described in Nomme et al. (2014). In brief, crystals of dCK in complex with UDP, $MgCl_2$, and a 2.5-fold excess of the DI-39 inhibitor were grown using the hanging drop vapor diffusion method at 12°C. The reservoir solution contained 0.9–1.5 M trisodium citrate dehydrate and 25 mM Hepes, pH 7.5. Diffraction data were collected at the Advanced Photon Source, Argonne National Laboratory on Life Sciences-Collaborative Access Team (LS-CAT) beamlines 21 ID-G.

Mouse xenograft tumor models and treatments. CEM xenograft tumors were developed in 8–12-wk-old female NSG mice by implanting $2 × 10^6$ CEM dCK[wt]-sGluc-GFP and/or dCK[low]-sGluc-GFP cells in 100 µl of equal volume Matrigel (BD) and RPMI s.c. in the flanks. Tumor growth was monitored daily by caliper measurements ([(length × width²)/2]) and blood *Gaussia* luciferase (GLuc) assay (Tannous, 2009). 10 µl of blood was collected via tail vein nick and mixed with 2 µl of 50 mM EDTA. 1 µl of blood was mixed with 99 µl PBS and transferred to a 96-well OptiPlate (Perkin Elmer). 100 µl of 20 µM coelenterazine substrate was mixed and luciferase activity was measured using a plate luminescence microplate reader SpectraMax L (Molecular Devices). Systemic tumor models were established by intravenous injection of 10^6 CEM dCK[wt]-sGluc-GFP or dCK[low]-sGluc-GFP in 100 µl RPMI. 2 g/kg dT was administered in saline and DI-39 in a mixture of 1.4% DMSO and 40% Captisol (Ligand Pharmaceuticals) mixture.

TUNEL assay. Tumors from CEM xenografts were harvested and fixed overnight in 10% buffered formalin solution. Samples were then paraffin-embedded and 5-µm sections were mounted on glass slides. TUNEL staining was performed according to the manufacturer's protocol (Roche). Stained slides were subsequently scanned on a ScanScope AT (Aperio) and analysis was conducted using Tissue Studio 64 (Dual) 3.5 (Definiens AG).

dCK kinase and uptake assays. These assays were performed as previously described (Shu et al., 2010).

Peripheral blood counts. All mice were anesthetized and whole blood was obtained through cardiac puncture. For peripheral blood counts, samples were collected in tubes containing EDTA and submitted to UCLA Division of Lab Animal Medicine for analysis.

PET imaging. PET/CT studies were performed as previously described (Radu et al., 2008; Shu et al., 2010).

Pharmacokinetic studies of DI-39 in mice. This assay was performed as previously described (Murphy et al., 2013).

Statistical analyses. All statistics are presented as averages of biological replicates with ±SEM, unless indicated. P-value significances were calculated from multiple replicates within a dataset representative of multiple independent experiments, as indicated, using one sample Student's *t* test function in Prism 5 (GraphPad Software).

Online supplemental material. Fig. S1 shows the FACS gating strategy to identify hematopoietic progenitor populations quantified in Fig. 8 (E and F). Table S1 shows data collection and refinement statistics for the DI-39-dCK crystal structure. Online supplemental material is available at http://www.jem.org/cgi/content/full/jem.20131738/DC1.

REFERENCES

Austin, W.R., A.L. Armijo, D.O. Campbell, A.S. Singh, T. Hsieh, D. Nathanson, H.R. Herschman, M.E. Phelps, O.N. Witte, J. Czernin, and C.G. Radu. 2012. Nucleoside salvage pathway kinases regulate hematopoiesis by linking nucleotide metabolism with replication stress. *J. Exp. Med.* 209:2215–2228. http://dx.doi.org/10.1084/jem.20121061

Bartek, J., M. Mistrik, and J. Bartkova. 2012. Thresholds of replication stress signaling in cancer development and treatment. *Nat. Struct. Mol. Biol.* 19:5–7. http://dx.doi.org/10.1038/nsmb.2220

Boulos, N., H.L. Mulder, C.R. Calabrese, J.B. Morrison, J.E. Rehg, M.V. Relling, C.J. Sherr, and R.T. Williams. 2011. Chemotherapeutic agents circumvent emergence of dasatinib-resistant BCR-ABL kinase mutations in a precise mouse model of Philadelphia chromosome-positive acute lymphoblastic leukemia. *Blood.* 117:3585–3595. http://dx.doi.org/10.1182/blood-2010-08-301267

Chiuten, D.F., P.H. Wiernik, D.S. Zaharko, and L. Edwards. 1980. Clinical phase I-II and pharmacokinetic study of high-dose thymidine given by continuous intravenous infusion. *Cancer Res.* 40:818–822.

Cohen, S., M. Megherbi, L.P. Jordheim, I. Lefebvre, C. Perigaud, C. Dumontet, and J. Guitton. 2009. Simultaneous analysis of eight nucleoside triphosphates in cell lines by liquid chromatography coupled with tandem mass spectrometry. *J. Chromatogr. B Analyt. Technol. Biomed. Life Sci.* 877:3831–3840. http://dx.doi.org/10.1016/j.jchromb.2009.09.030

Csapo, Z., G. Keszler, G. Safrany, T. Spasokoukotskaja, I. Talianidis, M. Staub, and M. Sasvari-Szekely. 2003. Activation of deoxycytidine kinase by gamma-irradiation and inactivation by hyperosmotic shock in human lymphocytes. *Biochem. Pharmacol.* 65:2031–2039. http://dx.doi.org/10.1016/S0006-2952(03)00182-5

Datta, N.S., D.S. Shewach, B.S. Mitchell, and I.H. Fox. 1989. Kinetic properties and inhibition of human T lymphoblast deoxycytidine kinase. *J. Biol. Chem.* 264:9359–9364.

de Bono, J.S., and A. Ashworth. 2010. Translating cancer research into targeted therapeutics. *Nature.* 467:543–549. http://dx.doi.org/10.1038/nature09339

Fong, P.C., D.S. Boss, T.A. Yap, A. Tutt, P. Wu, M. Mergui-Roelvink, P. Mortimer, H. Swaisland, A. Lau, M.J. O'Connor, et al. 2009. Inhibition of poly(ADP-ribose) polymerase in tumors from BRCA mutation carriers. *N. Engl. J. Med.* 361:123–134. http://dx.doi.org/10.1056/NEJMoa0900212

Hanahan, D., and R.A. Weinberg. 2011. Hallmarks of cancer: the next generation. *Cell.* 144:646–674. http://dx.doi.org/10.1016/j.cell.2011.02.013

Hastak, K., R.K. Paul, M.K. Agarwal, V.S. Thakur, A.R. Amin, S. Agrawal, R.M. Sramkoski, J.W. Jacobberger, M.W. Jackson, G.R. Stark, and M.L. Agarwal. 2008. DNA synthesis from unbalanced nucleotide pools causes limited DNA damage that triggers ATR-CHK1-dependent p53 activation. *Proc. Natl. Acad. Sci. USA.* 105:6314–6319. http://dx.doi.org/10.1073/pnas.0802080105

Jain, M., R. Nilsson, S. Sharma, N. Madhusudhan, T. Kitami, A.L. Souza, R. Kafri, M.W. Kirschner, C.B. Clish, and V.K. Mootha. 2012. Metabolite profiling identifies a key role for glycine in rapid cancer cell proliferation. *Science.* 336:1040–1044. http://dx.doi.org/10.1126/science.1218595

Jordheim, L.P., E. Cros, M.H. Gouy, C.M. Galmarini, S. Peyrottes, J. Mackey, C. Perigaud, and C. Dumontet. 2004. Characterization of a gemcitabine-resistant murine leukemic cell line: reversion of *in vitro* resistance by a mono-nucleotide prodrug. *Clin. Cancer Res.* 10:5614–5621. http://dx.doi.org/10.1158/1078-0432.CCR-04-0506

Kamphorst, J.J., J. Fan, W. Lu, E. White, and J.D. Rabinowitz. 2011. Liquid chromatography-high resolution mass spectrometry analysis of fatty acid metabolism. *Anal. Chem.* 83:9114–9122. http://dx.doi.org/10.1021/ac202220b

Kufe, D.W., P. Beardsley, D. Karp, L. Parker, A. Rosowsky, G. Canellos, and E. Frei III. 1980. High-dose thymidine infusions in patients with leukemia and lymphoma. *Blood.* 55:580–589.

Kufe, D.W., M.M. Wick, S. Moschella, and P. Major. 1981. Effect of high-dose thymidine infusions in patients with mycosis fungoides. *Cancer.* 48:1513–1516. http://dx.doi.org/10.1002/1097-0142(19811001)48:7<1513::AID-CNCR2820480705>3.0.CO;2-Q

Luo, J., N.L. Solimini, and S.J. Elledge. 2009. Principles of cancer therapy: oncogene and non-oncogene addiction. *Cell.* 136:823–837. http://dx.doi.org/10.1016/j.cell.2009.02.024

Maddocks, O.D., C.R. Berkers, S.M. Mason, L. Zheng, K. Blyth, E. Gottlieb, and K.H. Vousden. 2013. Serine starvation induces stress and p53-dependent metabolic remodelling in cancer cells. *Nature.* 493:542–546. http://dx.doi.org/10.1038/nature11743

Matsuoka, S., B.A. Ballif, A. Smogorzewska, E.R. McDonald III, K.E. Hurov, J. Luo, C.E. Bakalarski, Z. Zhao, N. Solimini, Y. Lerenthal, et al. 2007. ATM and ATR substrate analysis reveals extensive protein networks responsive to DNA damage. *Science.* 316:1160–1166. http://dx.doi.org/10.1126/science.1140321

Murphy, J.M., A.L. Armijo, J. Nomme, C.H. Lee, Q.A. Smith, Z. Li, D.O. Campbell, H.I. Liao, D.A. Nathanson, W.R. Austin, et al. 2013. Development of new deoxycytidine kinase inhibitors and noninvasive in vivo evaluation using positron emission tomography. *J. Med. Chem.* 56:6696–6708. http://dx.doi.org/10.1021/jm400457y

Nomme, J., J.M. Murphy, Y. Su, N.D. Sansone, A.L. Armijo, S.T. Olson, C. Radu, and A. Lavie. 2014. Structural characterization of new deoxycytidine kinase inhibitors rationalizes the affinity-determining moieties of the molecules. *Acta Crystallogr. D Biol. Crystallogr.* 70:68–78. http://dx.doi.org/10.1107/S1399004713025030

O'Dwyer, P.J., S.A. King, D.F. Hoth, and B. Leyland-Jones. 1987. Role of thymidine in biochemical modulation: a review. *Cancer Res.* 47:3911–3919.

Ooi, K., T. Ohkubo, M. Higashigawa, H. Kawasaki, and M. Sakurai. 1996. Increased deoxycytidine kinase activity by etoposide in L1210 murine leukemic cells. *Biol. Pharm. Bull.* 19:1382–1383. http://dx.doi.org/10.1248/bpb.19.1382

Radu, C.G., C.J. Shu, E. Nair-Gill, S.M. Shelly, J.R. Barrio, N. Satyamurthy, M.E. Phelps, and O.N. Witte. 2008. Molecular imaging of lymphoid organs and immune activation by positron emission tomography with a new [18F]-labeled 2′-deoxycytidine analog. *Nat. Med.* 14:783–788. http://dx.doi.org/10.1038/nm1724

Reichard, P. 1988. Interactions between deoxyribonucleotide and DNA synthesis. *Annu. Rev. Biochem.* 57:349–374. http://dx.doi.org/10.1146/annurev.bi.57.070188.002025

Schoppy, D.W., R.L. Ragland, O. Gilad, N. Shastri, A.A. Peters, M. Murga, O. Fernandez-Capetillo, J.A. Diehl, and E.J. Brown. 2012. Oncogenic stress sensitizes murine cancers to hypomorphic suppression of ATR. *J. Clin. Invest.* 122:241–252. http://dx.doi.org/10.1172/JCI58928

Schwarzenberg, J., C.G. Radu, M. Benz, B. Fueger, A.Q. Tran, M.E. Phelps, O.N. Witte, N. Satyamurthy, J. Czernin, and C. Schiepers. 2011. Human biodistribution and radiation dosimetry of novel PET probes targeting the deoxyribonucleoside salvage pathway. *Eur. J. Nucl. Med. Mol. Imaging.* 38:711–721. http://dx.doi.org/10.1007/s00259-010-1666-z

Shields, A.F., J.R. Grierson, B.M. Dohmen, H.J. Machulla, J.C. Stayanoff, J.M. Lawhorn-Crews, J.E. Obradovich, O. Muzik, and T.J. Mangner. 1998. Imaging proliferation in vivo with [F-18]FLT and positron emission tomography. *Nat. Med.* 4:1334–1336. http://dx.doi.org/10.1038/3337

Shu, C.J., D.O. Campbell, J.T. Lee, A.Q. Tran, J.C. Wengrod, O.N. Witte, M.E. Phelps, N. Satyamurthy, J. Czernin, and C.G. Radu. 2010. Novel PET probes specific for deoxycytidine kinase. *J. Nucl. Med.* 51:1092–1098. http://dx.doi.org/10.2967/jnumed.109.073361

Stella, V.J., and Q. He. 2008. Cyclodextrins. *Toxicol. Pathol.* 36:30–42. http://dx.doi.org/10.1177/0192623307310945

Tannous, B.A. 2009. *Gaussia* luciferase reporter assay for monitoring biological processes in culture and *in vivo*. *Nat. Protoc.* 4:582–591. http://dx.doi.org/10.1038/nprot.2009.28

Toy, G., W.R. Austin, H.I. Liao, D. Cheng, A. Singh, D.O. Campbell, T.O. Ishikawa, L.W. Lehmann, N. Satyamurthy, M.E. Phelps, et al. 2010. Requirement for deoxycytidine kinase in T and B lymphocyte development. *Proc. Natl. Acad. Sci. USA.* 107:5551–5556. http://dx.doi.org/10.1073/pnas.0913900107

Vander Heiden, M.G. 2011. Targeting cancer metabolism: a therapeutic window opens. *Nat. Rev. Drug Discov.* 10:671–684. http://dx.doi.org/10.1038/nrd3504

Warburg, O., F. Wind, and E. Negelein. 1927. The metabolism of tumors in the body. *J. Gen. Physiol.* 8:519–530. http://dx.doi.org/10.1085/jgp.8.6.519

Williams, R.T., M.F. Roussel, and C.J. Sherr. 2006. *Arf* gene loss enhances oncogenicity and limits imatinib response in mouse models of Bcr–Abl-induced acute lymphoblastic leukemia. *Proc. Natl. Acad. Sci. USA.* 103:6688–6693. http://dx.doi.org/10.1073/pnas.0602030103

Xu, Y.Z., P. Huang, and W. Plunkett. 1995. Functional compartmentation of dCTP pools. Preferential utilization of salvaged deoxycytidine for DNA repair in human lymphoblasts. *J. Biol. Chem.* 270:631–637.

Yang, C., M. Lee, J. Hao, X. Cui, X. Guo, C. Smal, F. Bontemps, S. Ma, X. Liu, D. Engler, et al. 2012. Deoxycytidine kinase regulates the G2/M checkpoint through interaction with cyclin-dependent kinase 1 in response to DNA damage. *Nucleic Acids Res.* 40:9621–9632. http://dx.doi.org/10.1093/nar/gks707

Yu, X.-C., M. Miranda, Z. Liu, S. Patel, N. Nguyen, K. Carson, Q. Liu, and J.C. Swaffield. 2010. Novel potent inhibitors of deoxycytidine kinase identified and compared by multiple assays. *J. Biomol. Screen.* 15:72–79. http://dx.doi.org/10.1177/1087057109353604